JOURNAL OF SOLID STATE CHEMISTRY 20, 245–256 (1977)

Inhomogeneous Transport at Low Temperatures in Alkali Halide Crystals

L. B. HARRIS

School of Physics, University of New South Wales, P.O. Box 1, Kensington, N.S.W. 2033, Australia

Received January 29, 1976; in revised form October 20, 1976

It is suggested that variation in the values obtained for the enthalpy of migration of a cation vacancy from measurements on NaCl and KCl is mainly due to the precision of experiments that is able to detect substructure differences between specimens. Evidence from previous work and from current observation indicates that extrinsic transport is basically inhomogeneous, and the existence of a substructure, and the presence of fast-ion transport within that substructure, is clearly demonstrated. A mechanism of localized transport arising from changes in impurity segregation to, and precipitation at, the substructure provides a consistent explanation, even in pure specimens, of observations on both conduction and diffusion.

1. Introduction

Our current understanding of conduction and diffusion in the alkali halides is not commensurate with the precision claimed for the experimental measurements (*1*). Although the defect mechanisms responsible for transport are well-established (*2*), there is considerable spread in the values deduced for the thermodynamic parameters associated with these mechanisms (*3*), as well as an incomplete fit between theory and experiment (*4*, *5*). It is appropriate, therefore, to seek factors not incorporated into present theory that might account for these deficiencies.

One factor almost invariably overlooked is specimen homogeneity, despite the fact that the defects contributing to transport, particularly the impurities contributing to extrinsic transport, are often not uniformly distributed (*6*). This lack of uniformity can, in certain circumstances, lead to structure-sensitive variations between specimens. The following sections give a brief summary of scatter in conduction and diffusion measurements in the extrinsic region for which no satisfactory explanation has been given, followed by an examination of data relating to specimen inhomogeneity. An account of recent observations then shows that inhomogeneous transport—transport in which ion flow varies from point to point within the specimen—is likely to be a factor responsible for at least part of the scatter previously described.

2. Reported Data

2.1. Conductivity Experiments

Measurements of conductivity, σ, as a function of absolute temperature T are usually presented as a conductivity plot of log σT against $1/T$, the original assumption (*7*) being that each straight-line segment of this plot is controlled by a single defect mechanism represented by a simple Arrhenius term. Each straight line slope, therefore, was expected to yield the enthalpy of the mechanism. In fact, extensive overlap of defect mechanisms (*8*, *9*) makes the fitting of data to theory a more complex process, but it can be adequately handled by a digital computer (*10*). Since intrinsic parameters are not uniquely determined by intrinsic conductivity data (*11*, *12*),

ISSN 0022-4596

a reliable computer fit requires conductivity measurements that extend into the cation extrinsic region, where a certain amount of impurity–vacancy pair formation is inevitable. Hence, a complete conductivity analysis involves the determination of eight unknown thermodynamic parameters: the enthalpies and entropies of Schottky defect formation, of anion and cation vacancy migration, and of impurity–vacancy association.

In this conductivity analysis the enthalpy of migration, $h_{m'}$, of a cation vacancy plays a key role, since the value assigned to it directly affects the values obtained for the enthalpy of Schottky formation and of association (*3*). It is therefore a matter of concern that the spread in values reported for h_m by different workers is much greater than the precision reported in each particular investigation. Early values obtained by fitting a straight line to region II of the conductivity plot (*13*) were too high, the unsuspected intrusion of association having increased the slope from one proportional to h_m toward one proportional to $h_m + h_a/2$, where h_a is an enthalpy of association. The presence of association is also the reason why computer analyses give values of h_m that are lower than those obtained graphically from region II. The logical conclusion is that, since association decreases with decrease in divalent impurity (*14*), the correct value is the lowest one, obtained in practice from a crystal sufficiently pure for the value obtained by computer to equal that obtained from the slope of region II. Results from actual measurements are, however, ambiguous.

Some observations on NaCl confirm a decrease in h_m with specimen purity. At a divalent impurity level of 10^{-6} mole fraction (m.f.), the slope of region II yielded a value of 0.68 eV, which was reduced by computer fitting to 0.65 eV (*3*), and increased by strontium doping toward 0.74 eV (*3*, *15*), while purer specimens with an effective impurity content of 5×10^{-8} m.f. yielded a value from the slope of region II of 0.63 eV (*16*). However, the value 0.74 eV is obtained graphically from many sets of observations on NaCl containing different dopants, including barium, cadmium, calcium, magnesium, nickel, and strontium (*3*, *8*, *17–21*), and is usually independent of the range of impurity concentration, so it cannot readily be rejected as a value artificially enhanced by association, particularly since other associative dopants in NaCl yield h_m values that are markedly lower (*22*, *23*). A further problem is that computer analysis is not always successful in separating migration and association parameters in doped specimens (*3*, *4*, *24*), which may partly account for an unusually high recently computed value for h_m of 0.81 eV (*21*). In pure NaCl ($<10^{-6}$ m.f. impurity) computer-derived values are 0.65 (*3*) and 0.715 eV (*24*).

Computer-derived values for h_m in KCl (*4*, *10*, *24–26*) range from 0.67 to 0.76 eV, but show no trend with specimen purity, while graphically determined values obtained on relatively pure samples are 0.67 (*4*), 0.77 (*27*),[1] 0.79 (*28*), and 0.81 eV (*29*), compared with 0.79 eV on strontium-doped KCl (*28*). The argument favoring the use of pure samples is sometimes put forward (*4*), although certain workers (*12*, *26*, *30*) advocate deliberate doping with divalent anions, as well as with cations, in order to produce distinct regions within which conductivity is dominated by a single type of lattice defect. Unfortunately, this latter technique introduces into the anion sublattice all the uncertainties associated with doping that have long been encountered in the cation lattice. In any case, owing to the limited solubility of anion impurities, it is usual to neglect association of these impurities with anion vacancies, a practice shown to introduce inaccuracies into the analysis (*31*). The use of very pure specimens also has problems, however, since extrinsic conductivity that is no longer completely dominated by divalent cations may show the anomalous influence of other factors, such as physical strain (*32*), trivalent or hydroxyl ions (*23*, *33*), or surface contamination (*34*, *35*).

2.2 Diffusion Experiments

According to simple theory the straight line diffusion plot of log D against $1/T$, where D is the cation self-diffusion coefficient, can be represented in the extrinsic region by an Arrhenius term in which the enthalpy is h_m

[1] Later recalculated as 0.81 eV (*29*).

(*15*, *36*, *37*). More generally a diffusion plot may be considered to yield an enthalpy of diffusion, h_D, which is equal to h_m only when association is negligible, a condition expected to occur in pure specimens. In practice, however, values of h_D in NaCl are not only larger than values of h_m obtained from conductivity but also tend to increase with an increase in specimen purity, which is in direct contrast with the decrease in h_m with purity described in Section 2.1. This increasing trend of h_D, clearly evident in Table I, has not been explained. The corresponding behavior in KCl has not been investigated, owing to the lack of a suitable potassium isotope.

Sometimes experimental data from both conductivity and diffusion measurements are incorporated in a single analysis (*25*, *30*, *38*), with the consequence that different values of h_m can be obtained from the same material depending on whether the analysis gives emphasis to diffusion in the cation or anion extrinsic region. In the case of KCl an analysis which linked conduction and diffusion in the cation extrinsic region yielded a value for h_m of 0.79 eV (*28*), whereas analysis which linked conduction in the cation extrinsic region with diffusion in the anion extrinsic region gave a value of 0.73 eV (*30*). This latter value is not necessarily better since the problems associated with working in the anion extrinsic region are not in principle less troublesome than those of the cation extrinsic region, merely less well known. This contradiction has not arisen with NaCl, since anion doping of this material is not practicable and the corresponding reduction in h_m from 0.72 (*15*) to 0.69 eV (*38*) is due simply to the assumed presence of association in region II.

2.3. Specimen Inhomogeneity

The spread in values quoted above contrasts with the regularity in results reported from any one laboratory, each of which has its own consistent set of values. Variations between laboratories must be mainly attributed to specimen variation, the one case of agreement, which concerns diffusion in NaCl (*39*, *40*), involving identical specimens similarly treated, i.e., as-received Harshaw crystals used without preanneal. Workers take care to avoid obvious perturbing influences on specimen behavior, such as contaminant (*1*, *12*), poor electrode contact (*3* *4*, *10*, *25*), and bulk precipitation (*4*, *10*), and then analyze results on the assumption that the impurity responsible for extrinsic transport is distributed uniformly throughout the crystal, whereas evidence from observations on precipitation suggests that this impurity is in fact segregated inhomogeneously. The precipitation region IV observed by conductivity (*7*) occurs at temperatures lower than those at which precipirates are observed by other techniques. In the case of calcium in NaCl, for example, the upper limit of region IV is near 420°K (7, *41*), whereas the corresponding density

TABLE I

ENTHALPY OF DIFFUSION h_D OF ^{22}Na IN NaCl DETERMINED FROM THE EXTRINSIC REGION OF DIFFUSION PLOTS

Specimen	Divalent impurity concentration (mole fraction $\times 10^6$)	h_D(eV)	Reference
strontium doped	27	0.72	(**15**)
pure	7	0.75	—[a]
Harshaw	?	0.77	(*36*)
purified salt	1	0.84	(*37*)
strontium doped	12	0.89	—[b]
pure	5	0.98	—[b]
pure	2	1.24	—[b]

[a] K. R. Riggs, Ph.D. Thesis, University of Missouri-Rolla (1970).

[b] F. Beniere and M. Chemla, *C.R. Acad. Sci. Paris 266C*, 660 (1968).

changes (*41*, *42*) and light scattering effects (*43*) reportedly extend up to 580°K (*44*). Precipitates resulting from 10^{-5} m.f. doping of Ca^{2+} in NaCl dissolve at 673°K only after an anneal of 18 hr (*45*), similar behavior being observed for precipitates in nominally pure NaCl (*46*) in which calcium is a common residual impurity. Other divalent impurities, including the commonly used dopant, strontium, also form precipitates at temperatures up to 673°K (*43*, *44*, *47*). One consequence is that h_m is often determined from conductivity measurements (*15*, *26*) in a temperature range that overlaps that in which precipitation has been observed (*24*, *47*), a matter usually disregarded provided precautions are taken and a suitable heating regime imposed on the specimen. However, just as association has been shown to be significant at temperatures as much as 300°K above the recognized association region (*9*, *24*), so also the effects of precipitation extend well above the precipitation region.

Precipitates nucleate preferentially at the specimen substructure of dislocations and subboundaries (*46*, *47*), and during thermal cycling they precipitate again at the sites at which they dissolved (*46*, *48*), which means that impurity segregates at and above the temperatures at which precipitates are observed, e.g., above the value of 673°K quoted above, as has been confirmed directly in the case of segregation to specimen surfaces (*49*). Compositional inhomogeneities resulting from crystal growth have been observed in doped (*50–52*) and pure (*52*) alkali halides and are exceptionally difficult to anneal out (*52*), probably because the local substructure of subboundaries at which precipitates nucleate are not changed significantly even by prolonged annealing near the melting point (*53*). In addition, certain pretreatments intended to stabilize the conductivity before an experimental run introduce strain and imperfections into the specimen. Annealing in situ (*3*, *10*, *25*), which uses plastic flow to bed the electrodes into the specimen, and thermal cycling (*24*), which introduces strain at thermal gradients and imperfections at the network of precipitation sites, establishes in the specimen a substructure at which preferential segregation (*54*) and precipitation (*44*) are likely to occur. Good specimen–electrode contact is essential, but it has been found that specimens fitted with electrodes satisfying all desirable criteria for good contact provide a wide spread in values of the region II slope that determines h_m (*55*).

If the effect of segregation is merely a rearrangement of cation vacancies without alteration in the number that contribute to transport, then the conductivity of the specimen will not change. Removal of vacancies by precipitation at the substructure as the temperature is reduced, below about 623°K in nominally pure NaCl (*45*, *46*), will, however, increase the slope of the conductivity plot. In pure crystals in which association and Debye–Hückel interactions (*14*) may be ignored, the slope changes from $-h_m/k$ to $-[h_m + h_p f/(f+1)]/k$, where h_p is an enthalpy of precipitation (solution) and f is the fraction of divalent impurity precipitated in the substructure. This mechanism is similar to the way in which bulk precipitation, at lower temperatures, increases the slope of region II and shortens its extent (*29*). The contraction of region II with the increase of purity (*8*, *15*) may in fact be due to precipitation of segregated residual impurity. Another possible mechanism, of a different kind, is localized fast-ion transport caused by phase-change disorder in the substructure. This would enhance σ and D (*56*), although decreasingly so with increasing temperature owing to desegregation, the net result being an apparent reduction in h_m. If this second mechanism occurs at higher temperatures than the first, then the overall effect of the substructure in the extrinsic region would be a slight (concave downwards) curvature. Nonrandom deviations in the computer fitting of conductivity data of both NaCl and KCl often have a curvature of this type (*3*, *10*, *25*). There are also instances of deviations in experimental data, such as conductivity hysteresis in pure NaCl near 623°K (*3*, *16*), additional components of conduction (*4*, *5*) and of diffusion (*39*), or an apparent deficiency of cation vacancies (*19*), where some effect of substructure appears to have been detected. Note that very slow cooling during conductivity

measurement (*3*, *4*), and the long annealing times required by diffusion experiments in the extrinsic region (*36*, *37*), tend to promote equilibrium segregation and phase-separation, while other experimental routines, such as the measurement of conductivity during heating (*19*, *20*), do not.

The precipitation observed in pure materials (*46*), even when divalent impurity is of the order of only 10^{-6} m.f. (*57*, *58*), is evidence that segregation persists even when overall impurity concentration is markedly reduced. Since association increases with impurity concentration (*14*), and is therefore greater in these segregated regions, it is probable that the ratio of the number of impurity–vacancy pairs in the substructure to the number of free vacancies in the specimen will increase with specimen purity. Since the cation vacancies in impurity–vacancy pairs contribute to diffusion but not to conduction, a simple explanation is provided of how h_D can increase with specimen purity while h_m decreases (Section 2.1).

In general, the effects on transport of segregation to a substructure are complex (*59*), the consequence being sometimes an increase and sometimes a decrease in transport (*60*), so it is necessary to look at experiments on the alkali halides that have attempted to investigate these effects directly.

2.4. Inhomogeneous Transport

A number of apparently incompatible observations have been made on the effect of substructure on transport. The introduction of grain boundaries into single crystals has been shown (*61*) to permanently increase the conductivity of pure NaCl, to increase the slope of region II, corresponding to an increase in h_m from 0.7 to 0.8 eV, and to extend association in doped NaCl to much higher temperatures, whereas the introduction of dislocations by deformation usually decreases extrinsic conductivity (*6*, *61*) while restoration requires a prolonged high temperature anneal (*61*). Both effects are attributed to a semi-permanent segregation and/or precipitation of divalent impurities and vacancies to the substructure. Dislocations as well as grain boundaries are found to increase the diffusion of anions (*62–64*), although the mechanism of enhancement has not been established, but there is flat disagreement as to whether they influence the diffusion of cations, some workers detecting no such influence (*64*, *65*), while others report a marked enhancement (*66*). A fast-transport substructure is not immediately detected by a diffusion experiment, since Fick's law continues to be obeyed (*56*, *64*), but the measured diffusion coefficient is larger than for a specimen without such a substructure. Cations injected into the substructure have been found to have a high mobility (*67*), but it is not clear whether this is also true of the selfcation of the host lattice.

There is more definite evidence concerning dc conduction. Selfdiffusion from a thin surface film of tracer gives a Gaussian penetration profile, so that a constant electric field applied during diffusion should shift the entire Gaussian profile into the specimen. However, undistorted tracer profiles are observed in NaCl only at temperatures above 973°K (*68*), measurements down to 873°K (*69*) producing asymmetrically distorted profiles due to regions of enhanced transport that developed into channels of electrode material extending from the anode. The formation of channels was attributed to imperfect electrode contact (*69*), but since identical electrodes gave satisfactory contact in diffusion experiments at the same temperature, it is more likely that the initial inhomogeneity was caused by injection of electrode material by the dc field. Such injection into dislocations (*67*) and grain boundaries (*70*), but not directly into the crystal lattice, takes place up to at least 863°K in LiF (*67*), the injected ions contributing to localized current and electrochemical decomposition in the substructure (*67*), possibly to local heating (*24*), and to enhanced values of σ.

3. Current Observations

3.1. Fast Transport Substructure

A number of observations in this laboratory on cation transport at extrinsic temperatures have a direct bearing on the problems raised

in previous sections. The complexities of these problems have made it necessary to concentrate on a simple substructure, a single plane grain boundary in a bicrystal, with reference back to behavior in single crystals wherever possible. Experimental techniques and detailed interpretation either have been, or will be, described elsewhere, the present aim being to summarize the results of observations which impinge on the inconsistencies described above.

Figure 1 shows the asymmetrical penetration profile typical of electrodiffusion experiments (diffusion in the presence of a dc field) on single crystals in the low temperature range 550–750°K, the form of the profile being similar for sodium and silver tracer in NaCl, and for potassium and silver tracer in KBr. The magnitude, x_m, of penetration at the profile maximum gives values of tracer mobility, μ, by means of the equation $x_m = \mu Et$, where E is the applied field and t is time of electrodiffusion (*68*), that agree with values of conductivity calculated from the average current through the specimen ($\sigma = ne\mu$, where n is the cation density and e is the electron charge). However, apparent values of the diffusion coefficient obtained by approximately

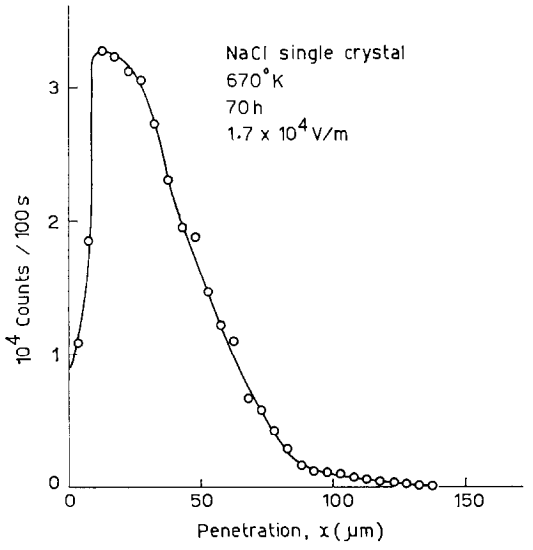

FIG. 1. Electrodiffusion tracer profile of ^{22}Na in single crystal NaCl at 670°K. 1.7×10^4 V/m applied for 70 hr.

fitting a Gaussian curve to the distorted profile are much larger than true D values obtained in a normal diffusion experiment. These results are similar to earlier ones at higher temperatures (*69*), but in the present case the mechanism of inhomogeneous transport can be demonstrated to be the injection of electrode ions. With the use of silver the preferential paths traveled by the injected ions become delineated by colloids of the silver metal, the identity of the colloid patterns with paths traveled by tracer having been established by autoradiography (*71*). Figure 2 shows tubular protruberances, each representing the boundary of a cloud of colloidal silver, penetrating from the anode into a single crystal to a maximum depth of 700 μm, the electrodiffusion tracer profile for this specimen being similar to that in Fig. 1, with a maximum at a penetration of 12.5 μm and a fast transport tail extending to 150 μm. Hence, the inhomogeneous transport shown in Fig. 2 can readily account for the asymmetrical distortion of Fig. 1, an explanation confirmed by experiments on bicrystals.

Figure 3 is a view, by dark-field microscopy of the plane of a grain boundary into which a large amount of silver (white) has been injected. This silver first developed as fine straight tendrils, stretching from the anode, that reached the cathode only 3 min after initial application of the field, followed by a build-up of the heavy spongy deposit observed near the cathode. A vertical pattern of faint lines still exists adjacent to the anode at the top of Fig. 3, although it is difficult to see except near the extreme right. This silver, directed preferentially along a one-dimensional array of boundary channels, represents fast-ion substructure transport (*57*). If the time taken for the silver colloids to reach the cathode is converted into a mobility, a value of 1.5×10^{-10} m^2/V-sec is obtained, which corresponds to a conductivity in the grain boundary region of 5×10^{-1} Ω^{-1}m^{-1}, comparable with that for good superionic conductors. The colloids of Fig. 3 are spread over a macroscopic boundary width of some 10 μm or more.

This technique of electrodecoration can reveal further aspects of injection. Figure 4

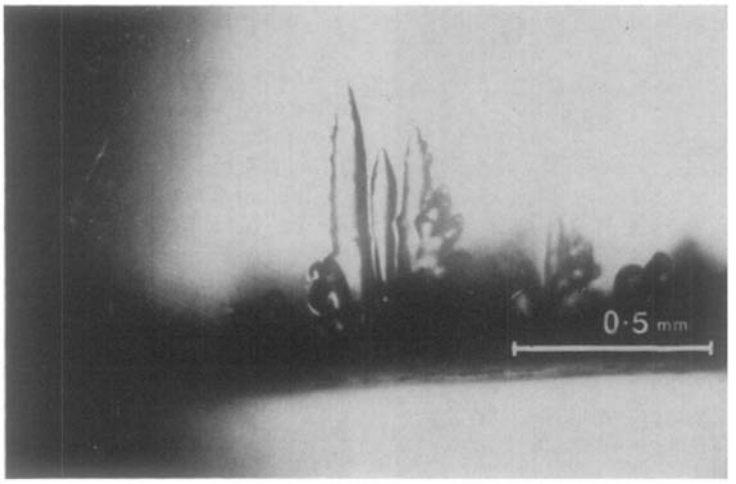

FIG. 2. Colloidal silver protrusions, extending upwards from anode surface, produced in NaCl crystal at 623°K by a field of 2×10^4 V/m applied for 200 hr; average current, 3 μA.

FIG. 3. Electrodecoration of a 10° KBr tilt boundary, viewed normal to the boundary plane between the anode (top) and the cathode (bottom); 1.5×10^5 V/m applied for 45 min at 473°K.

shows the cleaved anode surface of a KBr single crystal across which high fields (up to 10^6 V/m) were applied continuously for several days at 450°K. The region shown was outside the (earthed) silver anode, the white lines and patches representing silver that has moved under the influence of the small tangential component of the field. Most of this silver remained on the surface, but it has penetrated into the specimen along two subboundaries, observable as "tramlines" extending upwards from the word "electrode". These tramlines have a finite width, e.g., near the letter "A", caused by preferential penetration of silver along subboundary planes that do not coincide with the direction of the applied field. The other white lines are surface tracks of silver, some of which run along

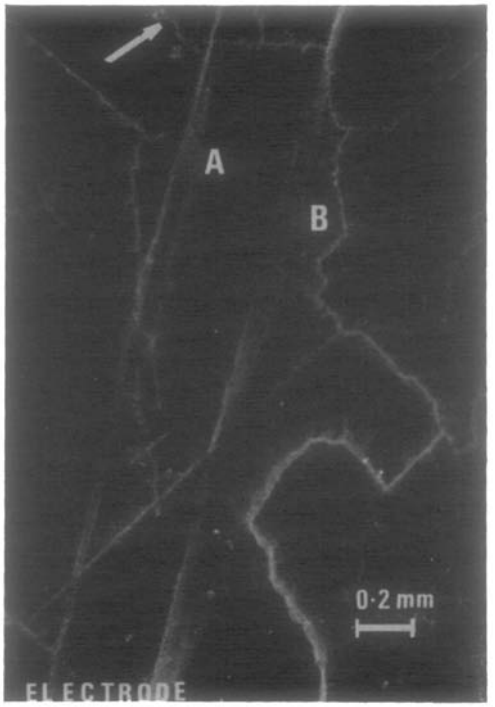

FIG. 4. High-field electrodecoration at 450°K on the cleaved surface of a KBr single crystal observed outside the anode electrode (bottom of micrograph). Silver has penetrated specimen along vertically slanting subboundaries (A, B), and at certain points along surface tracks, e.g., near the arrowhead.

cleavage steps at approximately 45° to the micrograph edges. Enlarged lambent blobs seen along these tracks, e.g., just above and below the apex of the arrow, are points at which the tracks penetrate into the solid under the influence of the main field across the specimen. The silver has tracked extensively over the surface under the small lateral component of the field, but has entered the specimen under the much larger main field at only a few selected points. The blobs and tramlines, with transport properties quite different from those of the bulk of the specimen, are part of the specimen's substructure. The fact that the observations in Fig. 4 were obtained on a surface not directly in contact with an electrode shows that transport inhomogeneity is a property of the specimen that has nothing to do with specimen–electrode contact.

3.2. Transport Mechanism

The high speed of injected cations has been attributed to dislocation pipe mobility (*67*). However, the fast transport represented by Figs. 1–4 has been shown to be independent of the existence of dislocations (*57*, *72*) and to be correlated rather with precipitates. Since the specimens of Figs. 2–4 are nominally pure, with a divalent impurity content between 10^{-5} and 10^{-6} m.f., precipitates of residual impurity are expected to be seen at the substructure (*73*). Figure 5 shows part of a pure NaCl 20° tilt boundary observed by scanning electron microscope in which geometrically shaped precipitates of different sizes are seen to be spread over a boundary width of at least 15 μm.

The way in which precipitation enhances transport is problematical. Electrodecoration colloids in bicrystals at lower temperatures (~473°K) are localized in tracks which appear to be sites of precipitate (*57*). The rapidity with which optically visible colloids (at least 1 μm in diameter) form along these tracks indicates that they are macroscopic regions over which extensive lattice rearrangement has taken place in a very short time. If at the temperature of electrodecoration the specimen substructure is not initially at segregation equilibrium or phase-separation equilibrium, then a change of order in the immediate vicinity of precipitate can provide the drive for the observed rapid transport. A residue of this disorder can apparently be frozen in, accounting for the increase in room temperature conductivity caused by precipitates in heavily doped NaCl (*74*, *75*). With an increase of electrodecoration temperature, the consequences of phase change are expected to become less locally intense, and it is correspondingly found that electrodecoration patterns above 600°K are coarsened and diffuse, although the colloids remain located within the grain boundary layer up to 773°K, indicating that segregation remains a factor of significance up to this temperature. The fact that the rate of electrodecoration above 600°K is less rapid than that near 500°K, resulting in an apparent negative activation enthalpy for transport, is almost certainly due

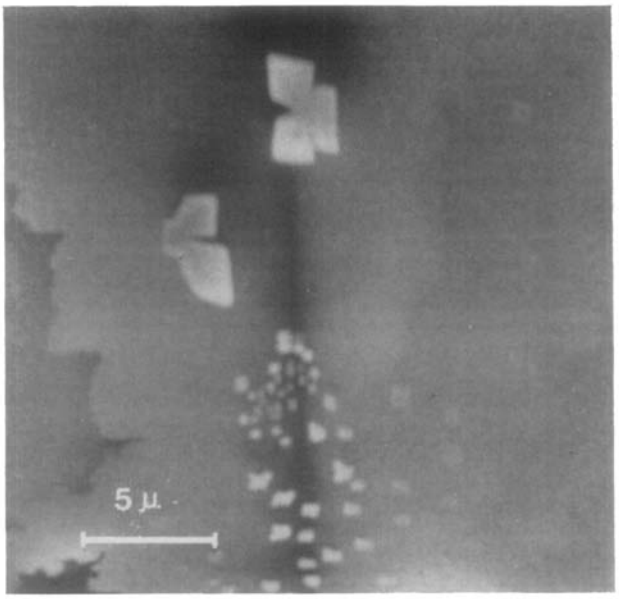

FIG. 5. Scanning electron micrograph of a NaCl 20° tilt boundary, looking along the boundary plane (vertical black line), showing the boundary precipitates (white).

to an increased rate of precipitation at the lower temperature. Thus the postulated second mechanism of Section 2.3, fast-ion transport associated with phase-change disorder and precipitation, operates in varying degrees over the entire upper extrinsic region.

It appears that the earlier experiments conceived as injection of ions into dislocation cores (*67*) should be reinterpreted as injection into diffuse regions of local disorder, similar to the injection that forms the blobs of Fig. 4. Injection into dislocations is unable to account for the formation by injected currents of large-scale dendritic structures (*67*), whereas it has been shown that continuous transport in the substructure produces substantial local erosion (*76*) able to accommodate such structures. The fact that electrodecoration colloids do not form readily in NaCl, as compared with KBr, makes it easier to recognize internal erosion in NaCl. Cathodic silver dendrites in the form of barbed spikes pointing against the field, as shown in Fig. 6, sometimes appeared suddenly in NaCl grain boundaries after the electrodecorating field had been applied for a considerable time. Such spikes are believed to be due to the reduction of silver ions, transported from the anode, by electrons injected from the cathode into an internal boundary surface produced by ion-transport erosion.

3.3. Substructure Diffusion

Electrodecoration is a more sensitive means of detecting inhomogeneous transport than radioactive tracer, the former always seeming to penetrate much further (cf. Figs. 1 and 2). Since there is little difference between the measured penetrations of silver tracer and sodium tracer, under similar experimental conditions it may be presumed, as a first approximation, that the observed penetration of silver colloids into the substructure also represents the (invisible) penetration of injected sodium ions. Certainly, Na^+ ions injected into NaCl bicrystals give rise to considerably enhanced boundary conduction (*77*). The question remains as to whether there is enhanced substructure transport in the absence of injection (*67*, *77*). It has been shown (*76*) that a dc field applied to NaCl bicrystals by noninjecting electrodes produces extensive electroerosion in the grain boundary region, but not elsewhere, which indicates preferential

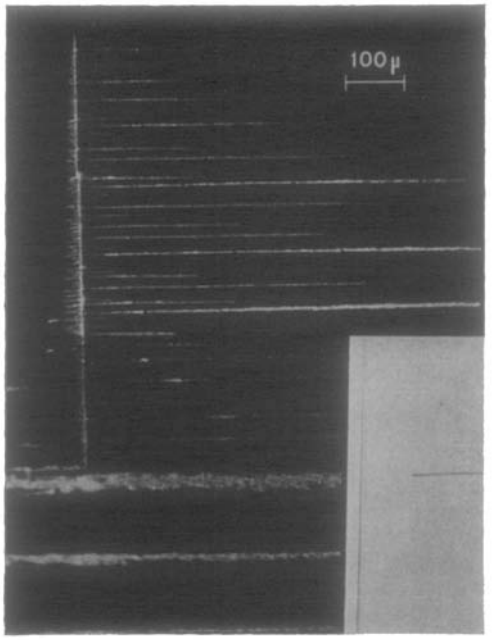

FIG. 6. Cathodic silver dendrite obtained in a NaCl 10° tilt boundary at 560°K after a field of 3.8×10^4 V/m had been applied (downwards) for 48 hr.

substructure transport. Since it may still be possible to regard such preferential transport as triggered by electrochemical decomposition at the electrodes, it is necessary to investigate what happens in diffusion when electrochemical effects are minimal.

Inhomogeneous transport in a diffusion experiment is identified by the presence of a tail on the penetration profile, similar to the long tail seen on the electrodiffusion profile of Fig. 1. Such tails have been detected (*78*, *79*) for the diffusion of sodium and silver into single crystals and bicrystals of NaCl, but only at short diffusion times ($\leqslant$70 hr at 633°K). At longer diffusion times the substructure diffusion is submerged by bulk diffusion in which case the presence of the substructure is not detected (*56*, *64*), apart from the indirect effect of an enhanced value of D. The annealing time in a cation diffusion experiment in the extrinsic region is usually much too long (*36*, *37*) for substructure transport to be detected, whereas annealing times in anion diffusion experiments, which use the ion-exchange technique (*62*, *63*), are very much shorter, e.g., 4 hr at 680°K for KBr (*63*). Since substructure effects show up more strongly at shorter times, this probably accounts for the apparent discrepancy between anion and cation diffusion mentioned earlier (Section 2.4).

Measurement of grain boundary diffusion determine values of the product $D'\delta$, where D' is the grain boundary diffusion coefficient and δ is grain boundary width. This product has been measured for sodium diffusion in NaCl and, depending on the value taken for δ, D' appears to be some two orders of magnitude greater than D (*78*). The transport width, δ, is large, between 1 and 10 μm (*78*, *79*), which agrees with other estimates (*59*, *80*), and which is entirely compatible with a substructure diffusion mechanism based on precipitation and segregation (cf. Fig. 5) as well as with the fact that electrodecoration colloids are spread over a layer about 10 μm wide. The larger the width of the substructure, the shorter the time in a diffusion experiment for a specimen to appear to be homogeneous (*56*). It has been shown (*79*) that annealing treatments that alter segregation to the grain boundary also alter the degree of enhancement of cation boundary diffusion and hence change the ratio of D' to D. By such annealing treatments it is possible to reconcile discrepancies with earlier workers (*64*, *65*). It is also found that cation boundary diffusion persists up to temperatures of at least 723°K (*79*), which shows that segregation influences diffusion over a temperature range similar to that over which it affects electrodecoration.

Recent work (*79*) has revealed considerable similarity between sodium and chlorine substructure diffusion in NaCl, both having a smaller activation enthalpy than bulk diffusion and both becoming progressively more significant at lower temperatures. In addition, anion substructure diffusion has a large width δ (*56*), tends at low temperatures to lead to apparently "homogeneous" diffusion in which anion D is enhanced (*62*), and is markedly influenced by high temperature annealing (*51*), all of which resembles cation diffusion behavior (*79*). There has even been an explanation of anomalous grain boundary diffusion in terms of a boundary phase change

(*81*). It is thus seen that similar mechanisms operate in the inhomogeneous transport of both anions and cations, leading to effects on diffusion and on dc conduction (as revealed by electrodecoration) that are entirely similar in kind. Hence, substructure fast-ion transport may be considered a general phenomenon.

Some apparent differences in behavior appear to be due to differences in the sensitivity of experimental techniques. Thus, electrodecoration of the grain boundary in Fig. 3 shows that certain ions have moved along this boundary some six orders of magnitude faster than ions in the bulk, whereas an experiment with radioactive tracer on the same boundary would reveal that ions at the tip of the tail in the penetration profile moved only about two orders of magnitude faster than those in the lattice. If it is required to know how far inhomogeneous transport in a specimen containing a substructure increases the conductivity above that in a specimen without substructure, then average behavior over all mobile ions is required, and the answer is now given by the average conductivity that will produce the distorted profile of Fig. 1 in place of the Gaussian profile of homogeneous conduction. The change in conductivity then becomes a good deal less than 100%, but sufficient to account for the order of scatter in h_m described in Section 2.1.

4. Conclusion

Inhomogeneous transport, in which specimen substructure contributes to variations in σ and D, has been shown to operate in both diffusion and dc conduction, primarily through the agency of segregated impurity. It therefore presumably also operates to perturb ac conduction, quite apart from any effect of electrochemical decomposition or electrode polarization. Inhomogeneous transport cannot exist in completely pure or completely homogenized specimens, but any state of nonequilibrium segregation during an experiment can introduce localized transport that can influence the measurement and affect the derived thermodynamic defect parameters, particularly those obtained from the cation extrinsic region. Similar effects are to be expected for anion impurity in the anion extrinsic region (*50*).

References

1. W. J. Fredericks, *in* "Diffusion in Solids" (A. S. Nowick and J. J. Burton, Eds.), p. 381, Academic Press, New York (1975).
2. R. G. Fuller, *in* "Point Defects in Solids" (J. H. Crawford and L. M. Slifkin, Eds.), Vol. 1, p. 103, Plenum Press, New York (1972).
3. A. R. Allnatt, P. Pantelis, and S. J. Sime, *J. Phys. C: Solid State Phys.* **4**, 1778 (1971).
4. P. W. M. Jacobs and P. Pantelis, *Phys. Rev.* **B4**, 3757 (1971).
5. N. Brown and P. W. M. Jacobs, *J. Physique* **34**, C9-437 (1973).
6. L. W. Barr and A. B. Lidiard, *in* "Physical Chemistry, An Advanced Treatise" (W. Jost, Ed.), Vol. X, p. 152, Academic Press, New York (1970)
7. R. W. Dreyfus and A. S. Nowick, *Phys. Rev.* **126**, 1367 (1962).
8. S. C. Jain and S. L. Dahake, *Indian J. Pure Appl. Phys.* **2**, 71 (1964).
9. C. Nadler and J. Rossel, *Helv. Phys. Acta* **44**, 937 (1971).
10. J. H. Beaumont and P. W. M. Jacobs, *J. Chem. Phys.* **45**, 1496 (1966).
11. D. K. Dawson and L. W. Barr, *Phys. Rev. Lett.* **19**, 844 (1967).
12. S. Chandra and J. Rolfe, *Canad. J. Phys.* **48**, 397 (1970).
13. R. W. Dreyfus and A. S. Nowick, *J. Appl. Phys. Suppl.* **33**, 473 (1962).
14. A. B. Lidiard, *in* "Handbuch der Physik" (S. Flugge, Ed.), Vol. XX, 2, p. 246, Springer-Verlag, Berlin (1957).
15. F. Beniere, M. Beniere, and M. Chemla, *J. Phys. Chem. Solids* **31**, 1205 (1970).
16. P. M. Gruzensky, *J. Chem. Phys.* **43**, 3807 (1965).
17. N. Brown and I. M. Hoodless, *J. Phys. Chem. Solids* **28**, 2297 (1967).
18. K. C. Kao, L. J. Giles, and J. H. Calderwood, *J. Appl. Phys.* **39**, 3955 (1968).
19. E. Laredo and E. Dartyge, *J. Chem. Phys.* **53**, 2214 (1970).
20. E. Laredo and D. Figueroa, *J. Physique* **34**, C9-449 (1973).
21. A. Mecseki, R. Voszka, L. Berkes, and I. Földvári, *Phys. Status Solidi (a)* **30**, K87 (1975).
22. S. J. Rothman, L. W. Barr, A. H. Rowe, and P. G. Selwood, *Philos. Mag.* **14**, 501 (1966).

23. D. L. KIRK AND P. L. PRATT, *Proc. Brit. Ceram. Soc.* **9**, 215 (1967).
24. C. NADLER AND J. ROSSEL, *Phys. Status Solidi(a)* **18**, 711 (1973).
25. R. G. FULLER, C. L. MARQUARDT, M. H. REILLY, AND J. C. WELLS, *Phys. Rev.* **176**, 1036 (1968).
26. S. CHANDRA AND J. ROLFE, *Canad. J. Phys.* **48**, 412 (1970).
27. H. GRÜNDIG, *Z. Phys.* **158**, 577 (1960).
28. M. BENIERE, F. BENIERE, AND M. CHEMLA, *J. Chim. Phys.* **67**, 1312 (1970).
29. G. KUMBARTZKI AND K. THOMMEN, *Z. Phys.* **184**, 355 (1965).
30. M. CHEMLA AND F. BENIERE, *J. Physique* **34**, C9–11 (1973).
31. H. J. WINTLE, *Philos. Mag.* **31**, 723 (1975).
32. H. KANZAKI, K. KIDO, AND T. NINOMIYA, *J. Appl. Phys. Suppl.* **33**, 482 (1962).
33. F. BENIERE AND R. ROKBANI, *J. Phys. Chem. Solids* **36**, 1151 (1975).
34. J. C. PENLEY, *J. Chem. Phys.* **45**, 756 (1966).
35. H. L. DOWNING AND R. J. FRIAUF, *J. Phys. Chem. Solids* **31**, 845 (1970).
36. D. MAPOTHER, H. N. CROOKS, AND R. MAURER, *J. Chem. Phys.* **18**, 1231 (1950).
37. R. REISFELD AND W. J. FREDERICKS, *Israel J. Chem.* **8**, 959 (1970).
38. M. BENIERE, M. CHEMLA, AND F. BENIERE, *J. Phys. Chem. Solids* **37**, 525 (1976).
39. S. J. ROTHMAN, N. L. PETERSON, A. L. LASKAR, AND L. C. ROBINSON, *J. Phys. Chem, Solids* **33**, 1061 (1972).
40. J. L. MITCHELL AND D. LAZARUS, *Phys. Rev.* **B12**, 734 (1975).
41. J. QUINN, B. A. W. REFERN, AND P. L. PRATT, *Proc. Brit. Ceram. Soc.* **9**, 35 (1967).
42. G. A. ANDREEV AND V. A. KLIMOV, *Sov. Phys. Solid State* **16**, 1926 (1975).
43. M. I. ABAEV AND M. I. KORNFEL'D, *Sov. Phys. Solid State* **7**, 2271 (1966).
44. G. A. ANDREEV AND V. A. KLIMOV, *Sov. Phys. Solid State* **16**, 1372 (1975).
45. M. NOTTIN, *Acta Cryst.* **A26**, 636 (1970).
46. M. GIRARD-NOTTIN AND L. TAUREL, *C.R. Acad. Sci. Paris* **260**, 4198 (1965).
47. G. HAURET AND M. GIRARD-NOTTIN, *Phys. Status Solidi* **17**, 881 (1966).
48. K. G. BANSIGIR AND E. E. SCHNEIDER, *J. Appl. Phys. Suppl.* **33**, 383 (1962).
49. M. J. YACAMÁN, *Phys. Status Solidi (b)* **56**, 429 (1973).
50. J. ROLFE, *Canad. J. Phys.* **42**, 2195 (1964).
51. L. W. BARR, J. A. MORRISON, AND P. A. SCHROEDER, *J. Appl. Phys.* **36**, 624 (1965).
52. A. R. ALLNATT AND A. V. CHADWICK, *Trans. Faraday Soc.* **63**, 1929 (1967).
53. J. WASHBURN AND J. NADEAU, *Acta Met.* **6**, 665 (1958).
54. A. J. R. DE KOCK, P. J. SEVERIN, AND P. J. ROKSNOER, *Phys. Status Solidi (a)* **22**, 163 (1974).
55. W. WHITHAM AND J. H. CALDERWOOD, *IEEE Trans. Elec. Insul.* **EI-8**, 61 (1973).
56. L. G. HARRISON, *Trans. Faraday Soc.* **57**, 1191 (1961).
57. L. B. HARRIS AND P. G. QUANG, *Phil. Mag.* **32**, 1213 (1975).
58. J. D. VENABLES, *J. Appl. Phys.* **34**, 293 (1963).
59. W. D. KINGERY, *J. Amer. Ceram. Soc.* **57**, 74 (1974).
60. C. M. OSBURN AND R. W. VEST, *J. Phys. Chem. Solids* **32**, 1355 (1971).
61. P. L. PRATT, *J. Physique* **34**, C9–213 (1973).
62. L. W. BARR, I. M. HOODLESS, J. A. MORRISON, AND R. RUDHAM, *Trans. Faraday Soc.* **56**, 697 (1960).
63. L. W. BARR AND D. K. DAWSON, UKAEA Report No. AERE-R 6234 (1969).
64. J. CABANE, *J. Chim. Phys.* **59**, 1135 (1962).
65. K. R. RIGGS AND M. WUTTIG, *J. Appl. Phys.* **40**, 4682 (1969).
66. YA.E. GEGUZIN, E. R. DOBROVINSKAYA, I. E. LEV, AND M. V. MOZHAROV, *Sov. Phys. Solid State* **8**, 2599 (1967).
67. R. TUCKER, A. LASKAR, AND R. THOMSON, *J. Appl Phys.* **34**, 445 (1963).
68. M. CHEMLA, *Ann. Phys.* **1**, 959 (1956).
69. V. C. NELSON AND R. J. FRIAUF, *J. Phys. Chem. Solids* **31**, 825 (1970).
70. R. L. MOMENT AND R. B. GORDON, *J. Appl. Phys.* **35**, 2489 (1964).
71. L. B. HARRIS AND J. L. SCHLEDERER *Acta Met.* **19**, 577 (1971).
72. L. B. HARRIS, *J. Crystal Growth*, in press.
73. L. B. HARRIS, D. A. MONCRIEFF, AND V. N. E. ROBINSON, *Phys. Status Solidi (a)* **35**, 371 (1976).
74. A. TOTH AND J. SARKÖZI, *Phys. Status Solidi (a)* **28**, K93 (1975).
75. A. TOTH AND J. SARKÖZI, *Phys. Status Solidi (a)* **30**, K193 (1975).
76. L. B. HARRIS, *J. Mater Sci.* **11**, 333 (1976).
77. K. G. MCQUHAE, Ph.D. Thesis, University of London (1969).
78. L. B. HARRIS AND J. FIASSON, *Phys. Status Solidi (a)* **33**, 697 (1976).
79. L. B. HARRIS, *J. Physique*, in press.
80. R. E. MISTLER AND R. L. COBLE, *J. Appl. Phys.* **45** 1507 (1974).
81. K. S. SABHARWAL, J. MIMKES, AND M. WUTTIG, *J. Appl. Phys.* **46**, 1839 (1975).